INTERFEROMETER SYSTEMS ON LHD

T. AKIYAMA,[a]* K. KAWAHATA,[a] K. TANAKA,[a] T. TOKUZAWA,[a] Y. ITO,[a] S. OKAJIMA,[b] K. NAKAYAMA,[b] C. A. MICHAEL,[c] L. N. VYACHESLAVOV,[d] A. SANIN,[d] S. TSUJI-IIO,[e] and LHD EXPERIMENT GROUP[a]

[a]*National Institute for Fusion Science, Toki 509-5292, Japan*
[b]*Chubu University, Kasugai 487-8501, Japan*
[c]*Culham Science Centre, Oxfordshire OX14 3DB, United Kingdom*
[d]*Budker Institute of Nuclear Physics, 630090, Novosibirsk, Russia*
[e]*Tokyo Institute of Technology, Meguro 152-8550, Japan*

Received July 16, 2009
Accepted for Publication October 28, 2009

This paper describes the interferometer systems on the Large Helical Device (LHD). LHD is equipped with five interferometer systems, each of which has a different operational purpose and measurable electron density range. A single-channel millimeter-wave interferometer is mainly used for low-density plasmas along a horizontal line of sight on the equatorial plane. Wavelengths of 1 and 2 mm are used for vibration compensation based on two-color interferometry, which has been used since the first operation of LHD. A 13-channel CH_3OH laser interferometer (wavelength of 119 μm) covers almost the whole poloidal cross sections of LHD plasmas with a chord separation of 90 mm. It routinely provides temporal behavior and profiles of the electron density. The laser has been developed as a collaboration between the National Institute for Fusion Science (NIFS) and Chubu University. An 80-channel CO_2 laser interferometer (10.6 μm) is employed for high-density plasmas such as superdense core plasmas. It adopts an imaging technique with three slablike beams and array detectors to measure the density profile precisely. A phase contrast imaging interferometer, which measures density fluctuations, is combined with the CO_2 laser interferometer. Since LHD has strong magnetic shear, a distribution of the density fluctuations is evaluated by using shear technique. A conventional millimeter-wave (4 mm) interferometer is also installed at a divertor region to measure dynamic density responses in a divertor leg. The phase counter used on these interferometers was originally developed at NIFS. The phase resolution of a typical phase counter is 1/100 fringe with a temporal response of 10 μs.

KEYWORDS: *LHD, interferometer, millimeter-wave, far-infrared and infrared laser*

Note: The figures in this paper are in color only in the electronic version.

I. INTRODUCTION

Since the line averaged electron density measured with an interferometer is indispensable for both plasma control and data analysis, interferometers are installed on almost all magnetic confinement fusion experimental devices. The interferometer is based on the simple principle that the phase difference ϕ between probe and reference beams depends on the electron density n_e since the refractivity N of the plasma is a function of the electron density.[1] In the case of *O*-mode, the relation between ϕ and n_e is as follows:

$$\phi = \frac{2\pi}{\lambda}\int (1 - N_o)\, dl = \frac{e^2}{4\pi\varepsilon_0 m_e c^2}\,\lambda \int n_e\, dl \ ,$$

where

λ = wavelength of the beam

e = charge of the electron

ε_0 = permittivity in vacuum

m_e = mass of the electron

c = velocity of light.

*E-mail: takiyama@lhd.nifs.ac.jp

When the interferometer operates at a relatively high electron density, it sometimes suffers from a measurement miss, called "fringe jump error." In the case of fast plasma density rise, the fringe jump occurs when the phase difference between two phase evaluations determined by sampling is larger than one fringe (2π). In addition, a strong electron density gradient causes refraction of the probe beam and leads to reduction of the detected signal intensity or even to temporary loss of the signal. Since the beam refraction is proportional to n_e and λ^2, fringe jump error is prone to happen in the high density and for a long-wavelength probe beam. In addition, the measured phase difference includes phase variation due to changes in the optical path length Δd caused by mechanical vibration. The phase errors $2\pi\Delta d/\lambda$ sometimes cannot be negligible.

These disadvantages can be alleviated by selecting an adequate wavelength for a probe beam and adopting compensation systems. Hence, the wavelength and the system should be determined according to the plasma parameters, device size, and purpose.

The Large Helical Device (LHD) is equipped with five interferometer systems, each of which has a different operational purpose and measurable electron density range. Section II describes concepts of interferometer systems on LHD. Section III is devoted to the details of each system, including recent measurement results. Section IV summarizes the systems reported.

II. INTERFEROMETERS ON LHD

The range of the electron density in LHD experiments is so wide, 10^{18} to 10^{21} m^{-3}, that interferometers with various wavelengths are necessary to obtain the density information with a high resolution and reliability. Three interferometer systems are operating on LHD for density control now: a millimeter-wave interferometer,[2] a CH_3OH laser interferometer,[3–5] and a CO_2 laser imaging interferometer.[6–11] The millimeter-wave interferometer with one horizontal chord on the midplane is used for density monitoring in the density range less than $\sim 5 \times 10^{19}$ m^{-3}. It has been working since the beginning of the LHD experiments. The 13-channel CH_3OH laser interferometer is the main interferometer on LHD. It routinely provides a density profile and is used for density feedback control. The CO_2 laser imaging interferometer is employed in the high-density range $>10^{20}$ m^{-3} since it is resistant to the fringe jump errors due to short wavelength. By adopting imaging scheme, the number of the detecting channels is large, and hence it can provide the detailed density profile.

Two specific interferometers are also operating: the phase contrast imaging (PCI) interferometer[12–19] and the divertor interferometer. The PCI is designed for plasma density fluctuation measurements.[20] Since magnetic configurations in LHD have strong magnetic shear in the peripheral region, the PCI on LHD can resolve the fluctuations spatially from line integrated measurements by using shear technique.[21] Although the standard measurable wavenumber range of fluctuations is 1 to 10 cm^{-1}, it can be extended toward small scales up to 30 cm^{-1} by modifications of the hardware.[17] The divertor interferometer is installed to measure the density in a divertor leg. It provides useful information of dynamic response of divertor plasmas, especially in case of divertor detachment experiments[22] and H-mode discharges.[23] These features of interferometers operating on LHD are summarized in Table I.

TABLE I

Features of Interferometers Installed on LHD

Interferometer	Characteristics	Density and Time Resolutions	Purpose
Millimeter	140 and 285 GHz, single channel, Mach-Zehnder	3.1×10^{15} m^{-3} (140 GHz) and 6.3×10^{15} m^{-3} (285 GHz), 10 μs	For relatively low density plasmas
CH_3OH laser	119 μm, 13 channels, Mickelson	5.6×10^{15} m^{-3} (central chord), 10 μs	Density profile measurement, density feedback
CO_2 laser imaging	10.6 μm and 1.06 μm (Nd:YAG laser for vibration compensation), 80 channels, Mach-Zehnder	1.1×10^{18} m^{-3} (central chord), 1 μs	For high-density plasmas (e.g., pellet-injected plasmas)
PCI	10.6 μm, magnetic shear technique, 2-D measurement with a 6×8 detector array	—	Measurement of density fluctuation profile
Divertor	66 GHz, single channel, Mach-Zehnder	2.3×10^{16} m^{-3} (supposing a pass length in a plasma 3 cm), 10 μs	Line density and density fluctuation measurement of divertor plasmas

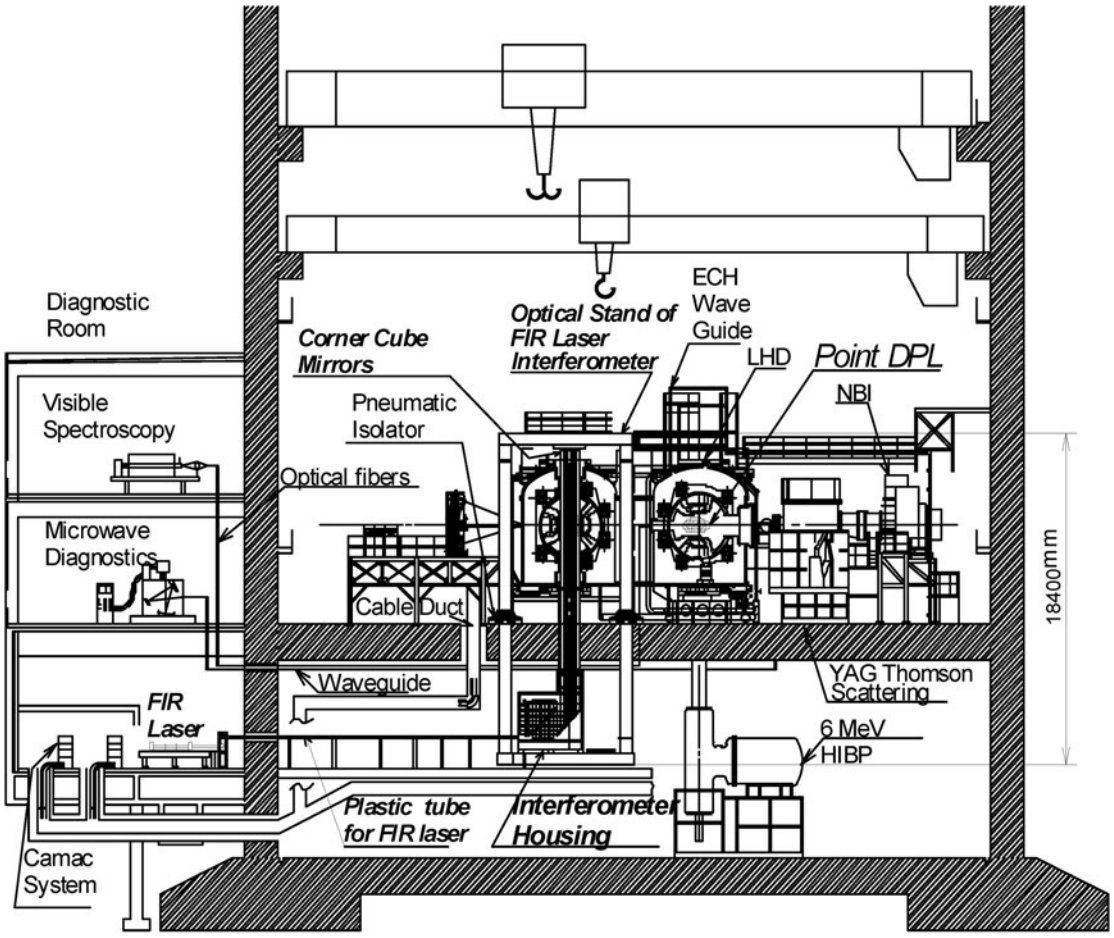

Fig. 1. Cross-sectional view of the LHD experiment hall and diagnostic rooms

III. PRESENT INTERFEROMETER SYSTEMS

Figure 1 shows a cross-sectional view of the LHD experimental hall and neighboring diagnostics rooms, including interferometer systems. The CH_3OH laser and Gunn oscillators are placed in the diagnostic rooms, which are behind a biological shield, a concrete wall with a thickness of 2 m. This is so that the system can be accessed to tune during plasma experiments. The beams are transmitted for more than 50 m using waveguides. The laser and components for the CO_2 laser interferometer are not shown in Fig. 1. They are placed above and below LHD on a vibration isolation frame. This is done to reduce vibration effects, which are severe in such a short-wavelength interferometer. The divertor interferometer also is not shown in Fig. 1. It is placed about 7 m away from LHD in the experiment hall.

III.A. Two-Color Millimeter-Wave Interferometer

The two-color millimeter-wave interferometer has been developed for the measurement of the line integrated electron density in the horizontal midplane of the LHD. Since the density measurement along the horizontal line of sight on the midplane is not affected by the Shafranov shift, it is suitable for average density monitor. Since the transmission path length (about 100 m) is so long that the effects of the change in path length would not be negligible during long-pulse plasmas up to 1 h, we have applied two-color interferometry at 140 and 285 GHz to compensate the changes in the path length.

Figure 2 shows a layout of the millimeter-wave interferometer on LHD. Gunn oscillators and quasi-optical (QO) circuits are placed in the diagnostic room and the wave is transmitted with a low loss HE_{11} corrugated waveguide, in which calculated transmission coefficients are about 78 and 93% at the frequencies of 140 and 285 GHz. To reduce the refractive effects caused by the density gradient, the interferometer chord is located in the horizontal midplane.

Figure 3 shows a block diagram of the interferometer with the QO system for 140 GHz. Phase-locked solid-state sources generate Gaussian beams with the power of 20 and 12 mW for 140 and 285 GHz, respectively. The

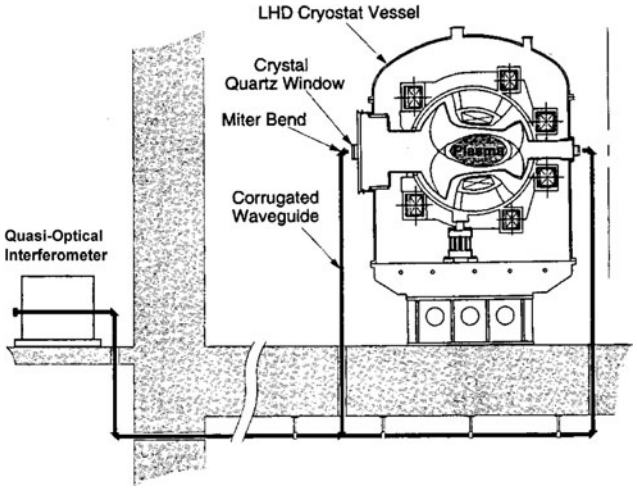

Fig. 2. Layout of the millimeter interferometer and LHD (from Ref. 2). Total path length of the probing wave is about 100 m.

two wavelength beams are overlaid with a Martin-Pupplet diplexer and are fed into the corrugated waveguide. After passing through a plasma, the waves go into the waveguide again and then back to the diagnostic room. Another diplexer separates the two wavelengths, and each is overlaid with corresponding local waves that have a frequency difference of 1 GHz for heterodyne detection. The frequencies of the millimeter waves of the signal and the reference are downconverted to an IF of 1 GHz with mixers. The superheterodyne receiver system that follows (not shown) compensates the drift of the IF and downconverts the IF to 1 MHz. The signals are input into a phase counter, whose phase resolution is 1/100 fringe with a frequency bandwidth of 100 kHz. The corresponding resolutions of the line averaged electron density are 3.1 and 6.3×10^{15} m^{-3} for 140 and 285 GHz (resolutions of the line density are 5.6 and 11.4×10^{15} m^{-2} for 140 and 285 GHz; the path length in a plasma is 1.81 m), respectively. Figure 4 shows an example of measurement

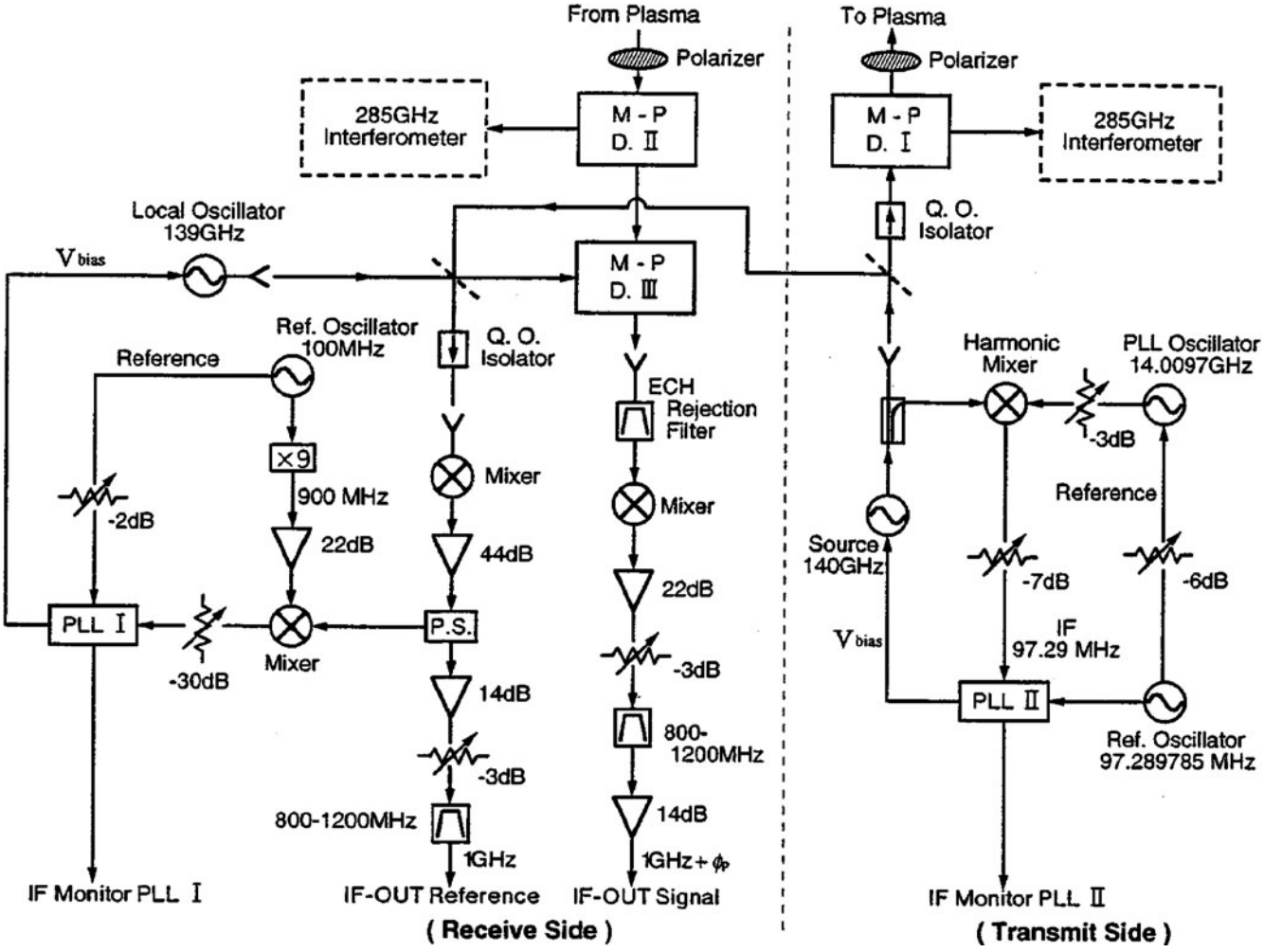

Fig. 3. Block diagram of QO circuits of the millimeter interferometer. Parts for 140 GHz only are drawn (from Ref. 2).

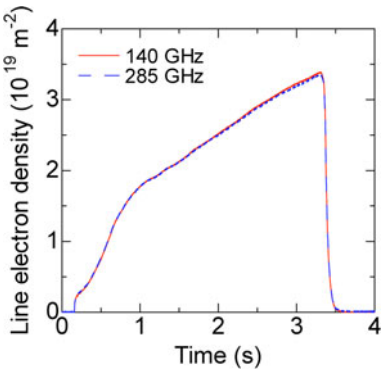

Fig. 4. An example of measurement results of the millimeter interferometer: 140 GHz (solid curve) and 285 GHz (dashed curve) (from Ref. 2).

results. The phase shift due to the change in the optical path length was found to be negligible. The line electron densities evaluated from each millimeter interferometer individually were almost the same, with a good signal-to-noise ratio. At present, it is not necessary to compensate the change in the optical path length. One of the millimeter interferometers is used as a backup system.

III.B. CH_3OH Laser Interferometer

The 13-channel far-infrared (FIR) laser interferometer system has been developed for the measurement of temporal behavior of the electron density profile on LHD. This is the main interferometer on LHD, and it is used also for feedback control of the electron density.

Of several candidates for FIR laser sources, the CH_3OH laser with a wavelength of 119 μm was taken as a probe beam from the viewpoints of output power level, small refraction effect, a high beat frequency, ease of maintenance, and gas handling. Figure 5 shows a schematic view of the CH_3OH laser jointly developed by the National Institute for Fusion Science and Chubu University. It is a twin laser system pumped by a continuous-wave CO_2 laser. One cavity length is feedback controlled to keep the output power at 90% of the maximum while the length of the other cavity is tuned to have a heterodyne beat frequency of 1 MHz between the two laser beams. Variations of the beat frequency are stabilized within $\pm$5 kHz, and the output

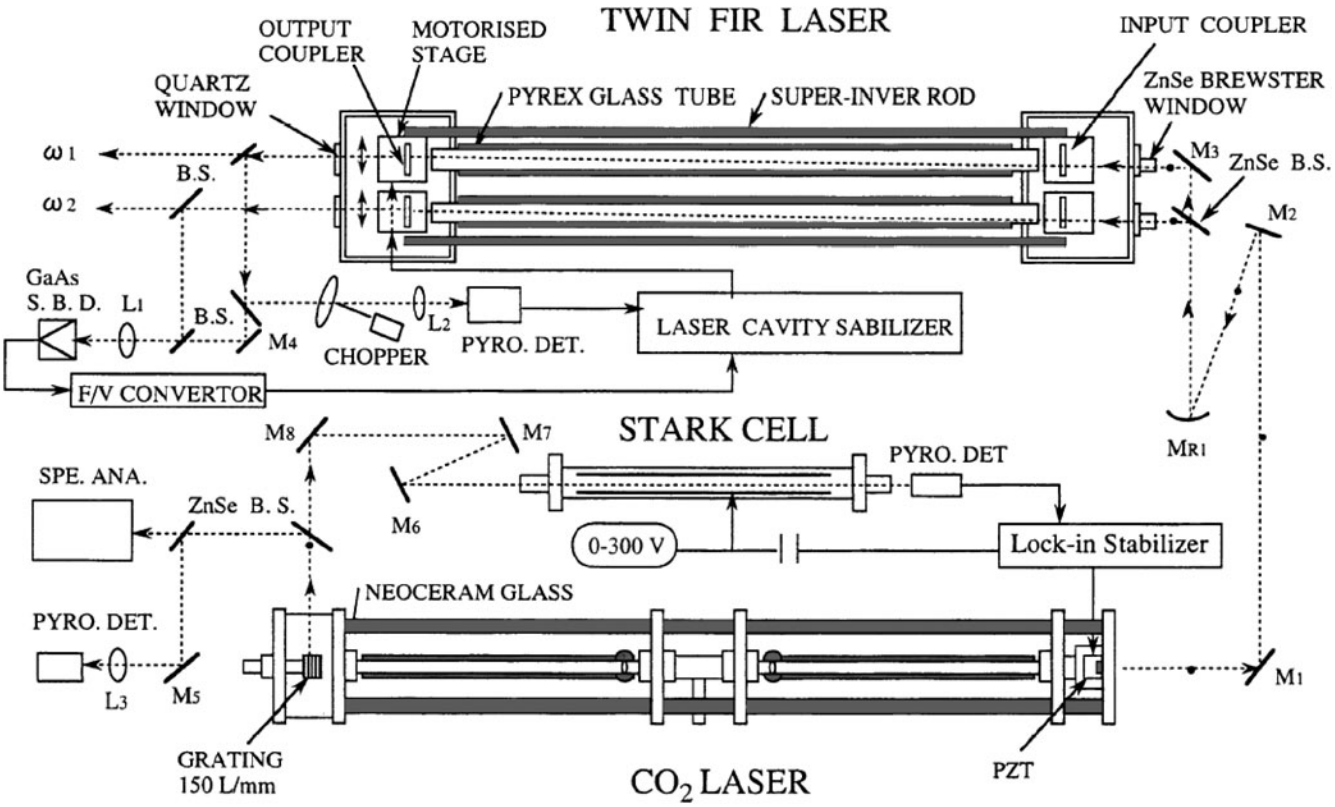

Fig. 5. Twin CH_3OH laser pumped by a CO_2 laser for the 13-channel interferometer on LHD (from Ref. 4). Total path length of the probing wave from the laser to a detector is about 80 m.

power is typically about 150 mW during plasma measurements.

The laser beams are transmitted for about 50 m from the laser toward the interferometer through dielectric waveguides made of an acrylic resin. To reduce absorption of the beam power by atmospheric water vapor, dry air flows along all the optical paths. The optical configuration is of the Michelson interferometer type with 13 channels, which cover almost the entire poloidal cross section. The chord spacing and the beam diameter are 90 and 50 mm, respectively. The optical system of the interferometer is mounted on a massive stainless frame floated on three vibration-isolating mounts. The resolution of the fringe counters is 1/80 fringe with a response time of 10 μs (Ref. 24), and it corresponds to a line averaged density of 5.6×10^{16} m^{-3} (a line density of 1.0×10^{17} m^{-2}; the path length in a plasma is 1.86 m) at the central chord, which is much smaller than the typical density range in LHD experiments (10^{19} to 10^{21} m^{-3}). The interferometer is equipped with a He-Ne laser interferometer for vibration compensation. However, the vibration isolation system damps vibrations well, and the amplitude is less than only 5 μm with a characteristic time of about 30 s. Hence, the phase errors due to mechanical vibrations are usually negligible even without compensation by the two-color interferometry.

Figure 6 shows an example of temporal behaviors of the line integrated densities and the reconstructed density profiles of a pellet-injected plasma.[5] In this density range, the rapid changes in the density can be measured without fringe jump errors. The density profiles are reconstructed with a slice and stack technique. The density profile is hollow during the electron cyclotron heating (ECH) phase and changes to the peaked one after pellet injection. The density gradient in the peripheral region becomes steeper when larger pellets are injected and the density rises up to 10^{20} m^{-3}. Fringe jump errors sometimes occur in such a high density range at the peripheral chords. For reliable measurements in the high-density plasma, the CO_2 laser interferometer, which is described next, has been developed.

III.C. CO_2 Laser Interferometer

As mentioned in the previous section, the CH_3OH laser interferometer sometimes suffers from fringe jump errors in the case of high-density plasmas by pellet injections. Since the beam-bending effect due to the density gradient is proportional to λ^2, the shorter wavelength is advantageous to avoid the errors. In addition, a normalized spatial resolution $\Delta R/a$ (ΔR is chord spacing and a is the minor radius) is typically $\sim$0.2 for the CH_3OH laser interferometer. Since LHD plasmas often have steep density gradient in the peripheral region, this spatial resolution is not sufficient for precise density profile measurements if one wants to understand details of particle confinement and instability.

Figure 7 shows schematic views of the CO_2 laser Mach-Zehnder imaging interferometer. The optics of the detection and transmission, shown in Figs. 7b and 7c, are placed below and above LHD, respectively. Since the wavelength is 10.6 μm, which is about 10 times shorter

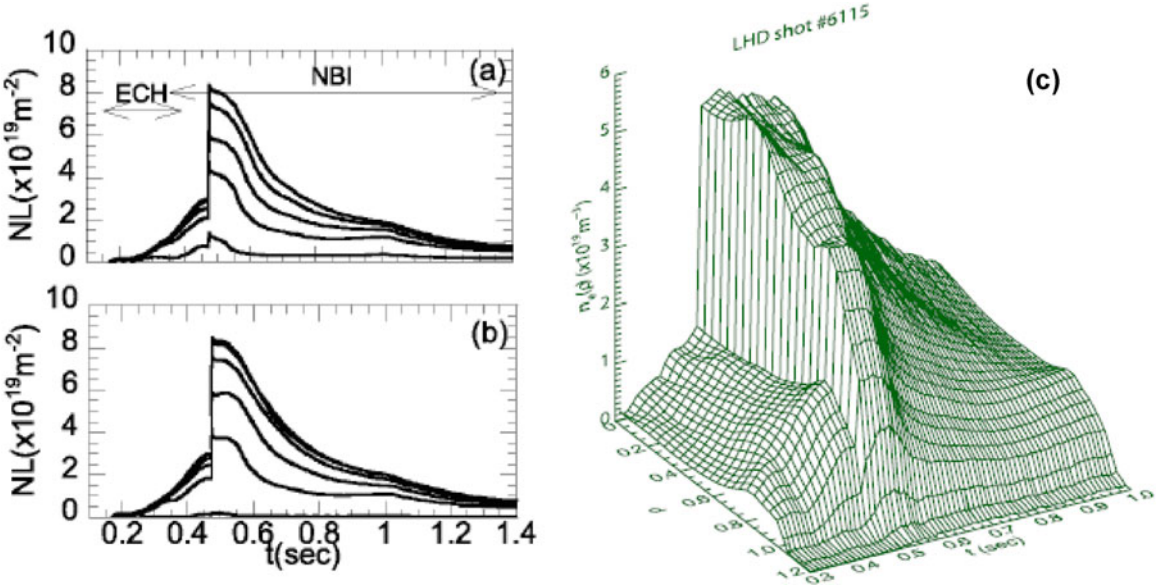

Fig. 6. Temporal behaviors of line integrated densities (a) at $R = 3.309$, 3.399, 3.489, 3.579, and 3.669 m (bottom to top) and (b) at $R = 3.759$, 3.849, 3.939, 4.029, 4.119, and 4.209 m (top to bottom). (c) Reconstructed density profiles measured with the CH_3OH laser interferometer (from Ref. 5).

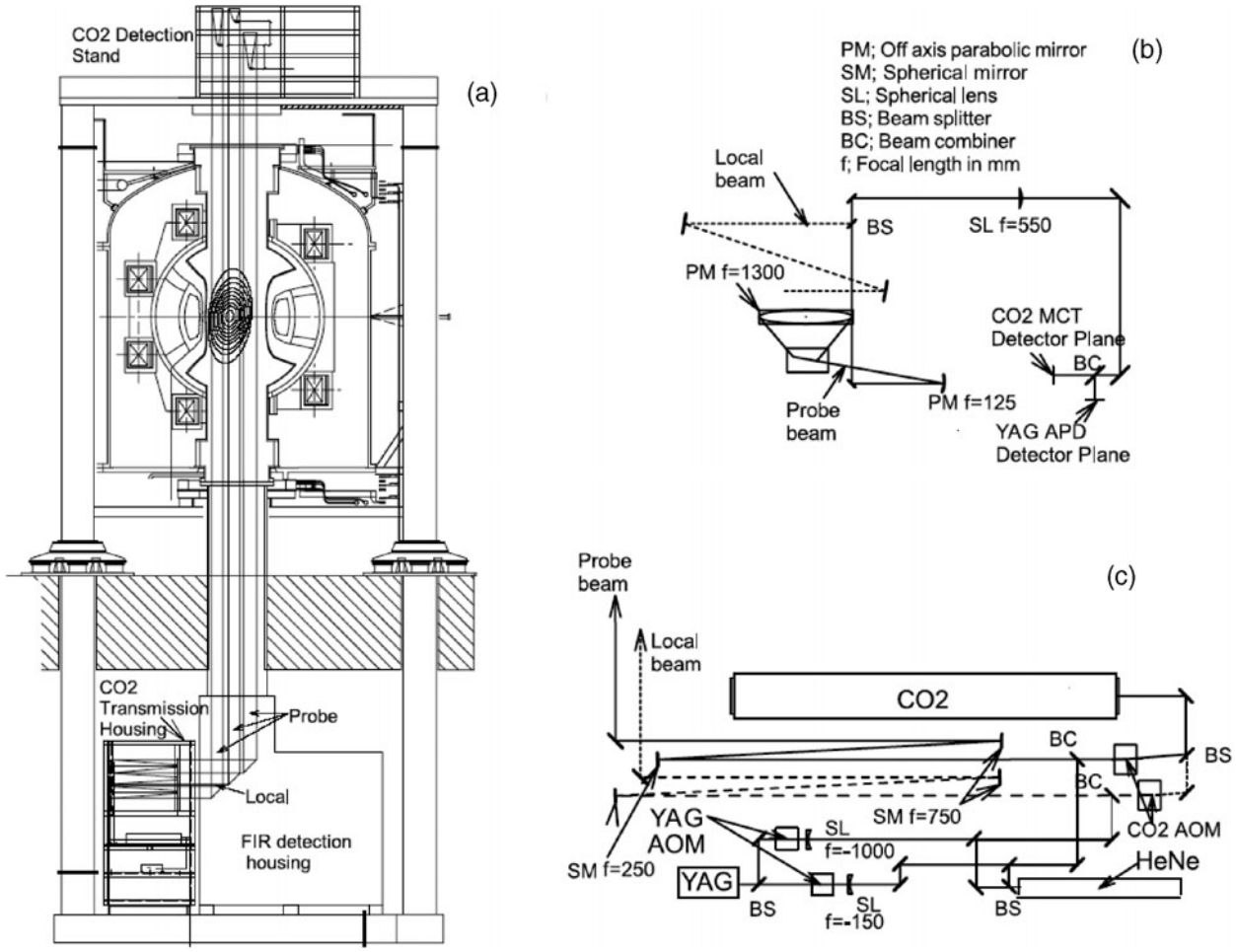

Fig. 7. (a) Schematic view of the CO_2 laser interferometer on LHD, and optical layouts of the (b) detection and (c) transmission systems (from Ref. 11). Total path length of probing beams is about 30 m.

than that of the CH_3OH laser, the beam-bending effect is two orders smaller than that of the CH_3OH laser; hence, the probability of fringe jump errors becomes smaller. The calculated beam displacement at the detection system is ~0.1 mm even in the case of an electron density profile of $1 \times 10^{20}\ (1 - \rho^2)\ \mathrm{m}^{-3}$. On the other hand, a short-wavelength interferometer is strongly affected by the mechanical vibrations. Hence, the optical system, including the CO_2 laser, is placed on the vibration isolation bench together with the CH_3OH laser interferometer. In addition, a continuous-wave Nd:YAG laser (1.06 μm) interferometer is introduced to compensate the mechanical vibrations. To improve the radial spatial resolution of the CO_2 interferometer, an imaging technique with three one-dimensional (1-D) detector arrays and slablike probe beams (cross section of the beam is 280×50 mm) is utilized. The total number of detector elements is 80 channels. Chordal resolution is from 15 to 22.5 mm, which depends on the slablike beams. Resolution of the line density is $2.1 \times 10^{18}\ \mathrm{m}^{-2}$ (a resolution of the line averaged electron density along the central chord of $1.1 \times 10^{18}\ \mathrm{m}^{-2}$, supposing the path length in a plasma is 1.85 m) with a response time of 1 μs.

Figure 8a shows the evolution of line integrated densities of a superdense core (SDC) plasma. Even though the density is increased by multi-injected pellets up to $3 \times 10^{20}\ \mathrm{m}^{-3}$ along the central chord, the interferometer can measure the density without fringe jump errors. The reconstruction of the profile from the line integrated density is done by using linear least-square fitting with regularization of the density gradient. These techniques are well established for tomography reconstruction. The reconstructed electron density profiles and comparison with the profiles obtained with the YAG laser Thomson scattering measurement are shown in Figs. 8d and 8e. It should be noted here that data points of the Thomson scattering measurement are relatively calibrated with Raman or Rayleigh scattering measurement, and the absolute value of the profile is determined to be consistent with the line averaged density

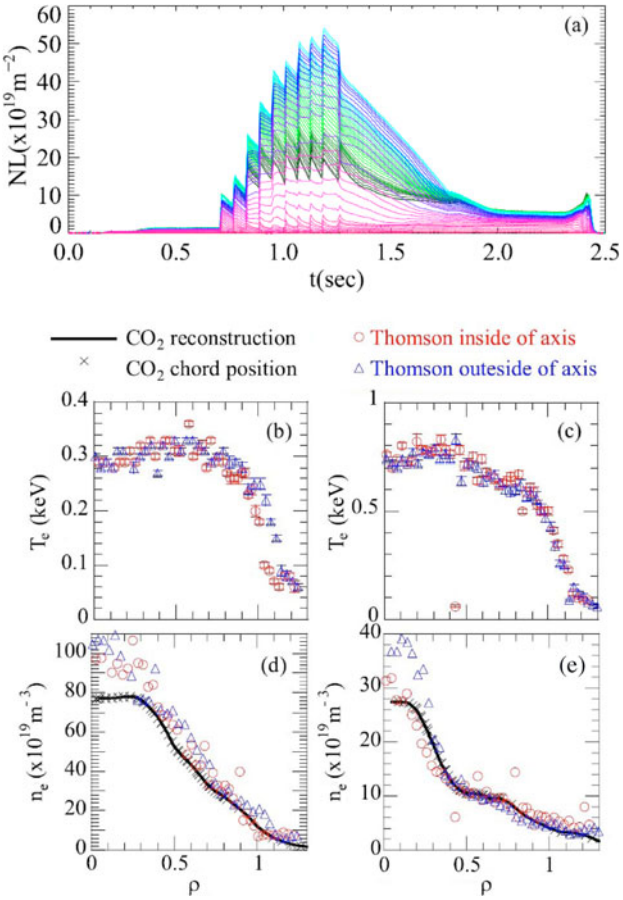

Fig. 8. (a) Evolution of line integrated densities of an SDC plasma, (b) and (c) electron temperature profiles, and (d) and (e) comparisons between density profiles measured with the CO_2 laser interferometer and the Thomson scattering measurement. (b) and (d) $t = 1.2$ s, (c) and (e) $t = 1.7$ s (from Ref. 11).

measured with the millimeter-wave interferometer. Density profiles agree well except in the core region $\rho < 0.3$. The reason for the disagreement in the core region is under examination.

III.D. PCI Interferometer

Since early systems of the PCI interferometer used 1-D detector arrays, the measurements were line integrated values. Even if the shear technique[21] was introduced, shot-by-shot adjustment of the detector angle was necessary to obtain the spatial profile of fluctuations. A two-dimensional (2-D) PCI with a 6×8 detector array, which can provide spatial fluctuation profile within a single discharge, has been developed on LHD. The laser and some optics for beam transmission are common with the CO_2 laser interferometer. The path of the probe beam is shown in Fig. 9. Taking advantage of strong magnetic

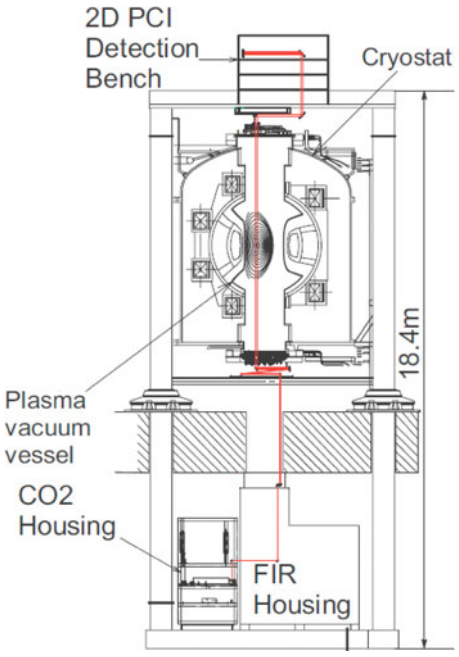

Fig. 9. Cross-sectional view of the phase contrast imaging interferometer on LHD (from Ref. 18). Total path length of the probing beam is about 30 m.

shear up to about ± 50 deg at the edge region, the shear technique makes it possible to resolve the fluctuations spatially with the single probe beam. The present measurable wave number region is 1 to 10 cm^{-1}, which is expected to be in the ion temperature gradient–driven instability region for LHD.

Measurements of a confinement-improved mode shown in Fig. 10 well demonstrate the capability of the 2-D PCI. H_α emission intensity spontaneously drops at $t = 2.51$ s under constant heating and fueling, whereas the line densities and the stored energy start to increase after the H_α drop. These behaviors indicate that particle confinement transits into improved mode. Figure 10c shows the change in the phase velocity of fluctuations measured with the 2-D PCI. In the peripheral region $1.1 < \rho < 1.3$, where a plasma is still confined by the thick ergodic layer (see Figs. 10d and 10e), the propagation direction changes from ion to electron diamagnetic after the transition. The spatial profiles of fluctuation powers and phase velocities before ($t = 2.3$ s) and after ($t = 2.7$ s) the transition are shown in Figs. 10f and 10g and Figs. 10h and 10i, respectively. The measured phase velocity includes $E_r \times B_t$ rotation of the plasma in the ion and electron diamagnetic directions, corresponding to the positive and negative E_r. It is possible that the reversal of the propagation direction after the transition might be attributed to the change in the radial electric field to negative, although the relationship among the density fluctuation, the electric field, and the transition is under study.

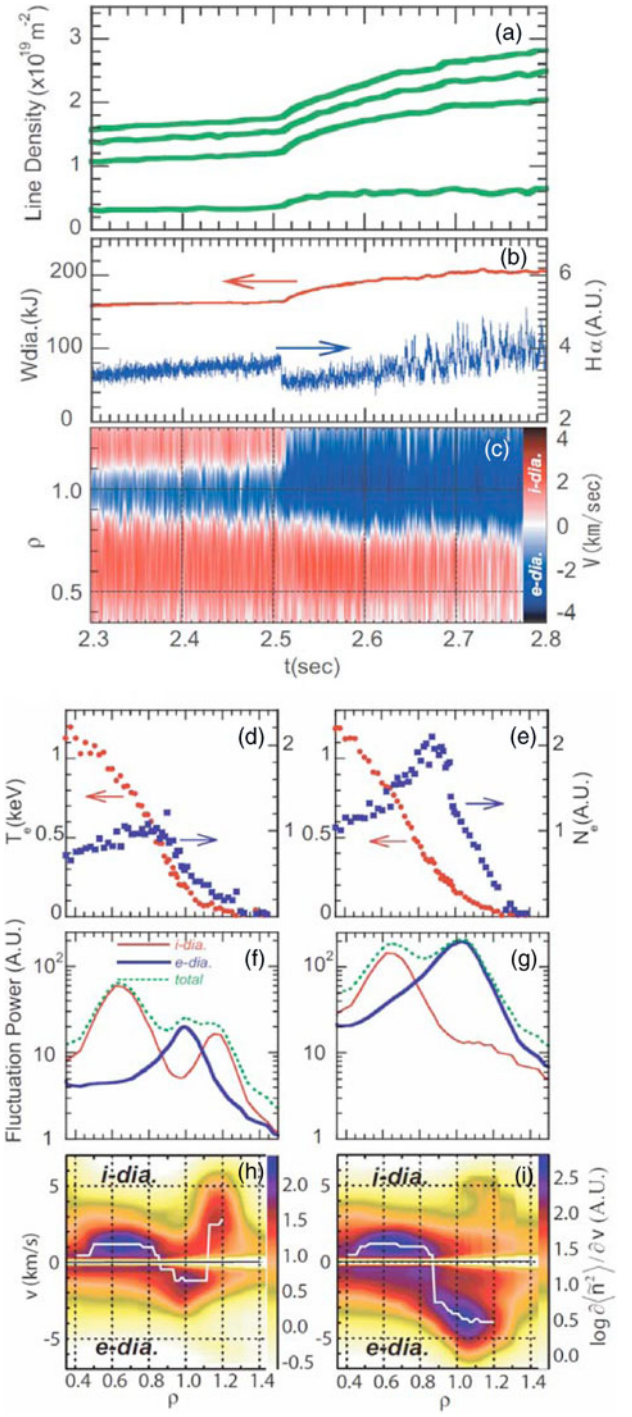

Fig. 10. H-mode discharge in LHD: (a) Line densities measured with CH_3OH laser interferometer (top to bottom, chord positions at the equatorial plane are ρ = 0.34, 0.58, 0.81, and 1.05). (b) H_α emission intensity and stored energy. (c) Phase velocity measured with 2-D PCI. (d) and (e) Electron temperature and density profiles. (f) and (g) Spatial profiles of fluctuation powers. (h) and (i) Spatial profiles of the phase velocity. (d), (f), and (h) and (e), (g), and (i) are before (t = 2.3 s) and after (t = 2.7 s) the H-mode transition, respectively (from Ref. 18).

III.E. Divertor Interferometer

One of the important issues in development of a fusion reactor is optimization of the divertor. To protect divertor plates from excessive power load, understanding and controlling the divertor plasma are necessary. Besides, the divertor plasma is sensitive to changes in confinement, for example, at H-mode transition or during magnetohydrodynamic (MHD) events; after transition to the H-mode, the divertor flux is expected to reduce due to confinement improvement and MHD events such as edge-localized modes flushing heat and particles to divertor. Hence, measurements of the divertor plasma would give physical insights even to core plasma behavior.

Langmuir probes (embedded probes in the divertor plates and reciprocating probes) are operated in LHD (Ref. 25). In addition to these diagnostics, direct measurements of the electron density by an interferometer with a good temporal resolution is useful for analysis of behavior of divertor plasmas and for modeling. Since the divertor plasma in LHD is so thin (about several centimeters) that it is difficult to measure with the interferometers described above, a millimeter-wave interferometer dedicated to measurements of the divertor plasma is installed.

Figure 11a shows a layout of circular waveguides in LHD. Transmitter and receiver antennas are installed near the outer and upper divertor leg on a cross section of the horizontally elongated plasma. An aluminum plate over the divertor leg, which is attached to another waveguide for the ultrashort-pulse reflectometer, reflects the millimeter wave to make a double path in the plasma.

A diagram of the components of the interferometer is shown in Fig. 11b. The frequency band and the output power of the Gunn oscillator used are from 63 to 70 GHz and larger than 16 dBm, respectively. The wide frequency band of the oscillator is intended for electron cyclotron absorption measurement. When the frequency of the wave matches with the electron cyclotron frequency f_c (GHz) = 28B (T) in the magnetized plasma, the wave is absorbed, and the amount of absorption depends on $n_e T_e$. Therefore, T_e can be evaluated from the absorption and measurement results of the interferometer. Since the magnetic field strength at the measurement position varies depending on the magnetic configuration, wide frequency range for the oscillator is preferable. The interferometer is a typical heterodyne one with an IF of 1 GHz. The superheterodyne receiver system similar to that in the millimeter-wave interferometer described in Sec. III.A is used. The phase counter is the same as that used in the CH_3OH laser interferometer. Although the electron density is less than several units of 10^{18} m^{-3} at the measurement position, the resolution of the line averaged density is 2.3×10^{16} m^{-3}, supposing that the path length in a divertor plasma is 3 cm (the line density is 6.9×10^{14} m^{-2}), with a response time of 10 μs.

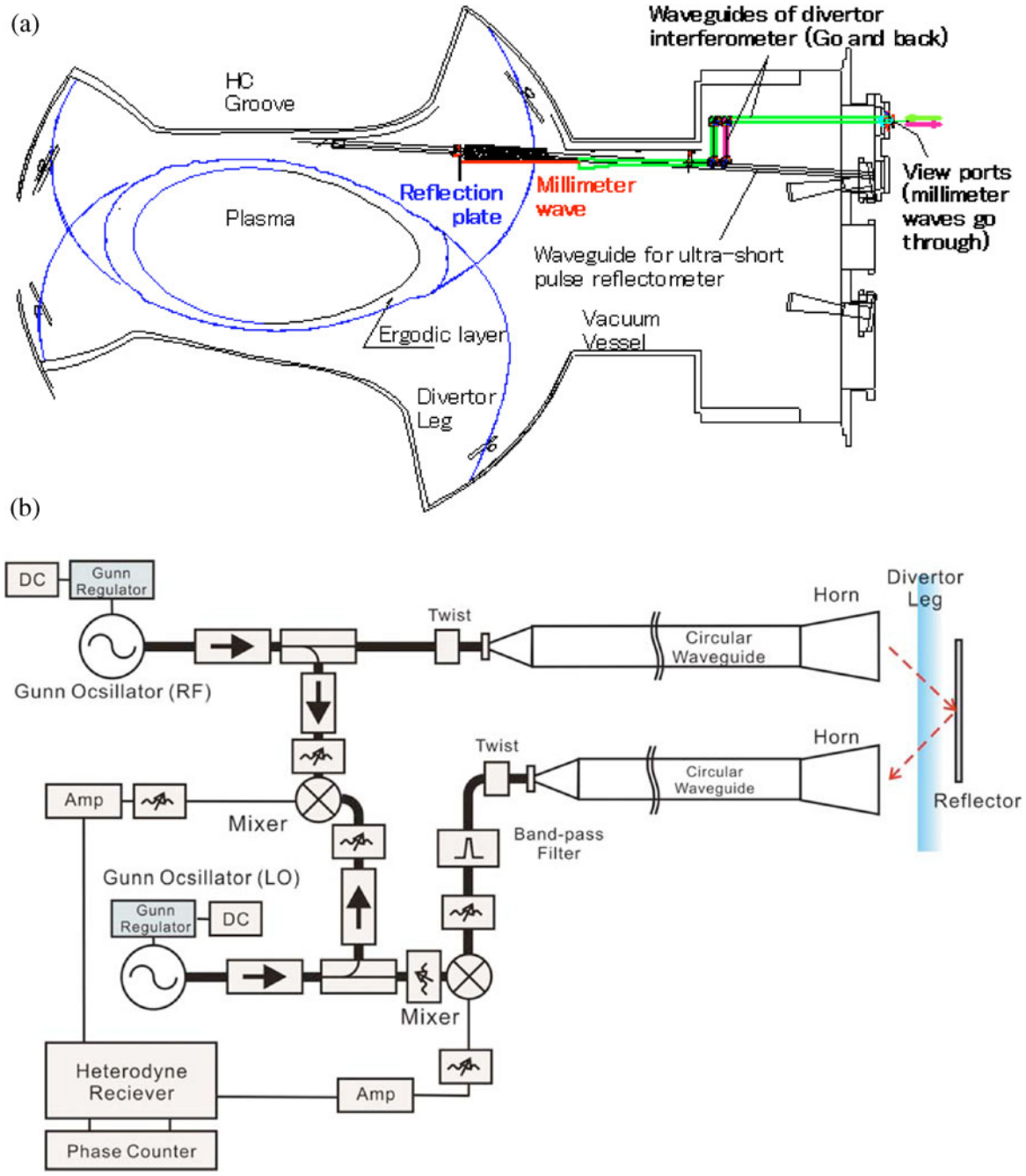

Fig. 11. (a) Cross section of the vacuum vessel and a plasma with the layout of the waveguides. (b) Diagram of millimeter-wave components of the interferometer. Total path length of the probing beam is about 20 m.

Figure 12 shows one example of the evolution of the divertor density. This is a detachment discharge, called "Serpens mode."[22] The density is rapidly increased by the short massive gas puff from $t = 2.0$ s, and then the plasma detached at $t = 2.1$ s. Density spikes, which correlated with the rotational radiation belt, are clearly observed.

IV. SUMMARY

The density range of LHD experiments is so wide that LHD is equipped with three interferometers; wavelengths are in the millimeter, FIR, and infrared regions for measurements in relatively low density, wide density, and high density ranges, respectively, to measure reliably

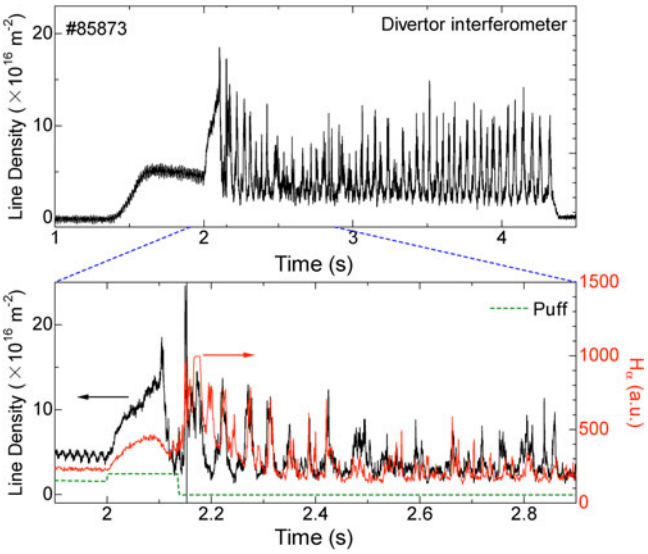

Fig. 12. One example of temporal behavior of the divertor density of self-sustained complete detachment discharge "Serpens mode."

(to avoid the fringe jump errors) with a high density resolution. The millimeter-wave interferometer has a horizontal line of sight on the midplane, which is suitable for the density monitor. The FIR (CH_3OH) laser interferometer has 13 channels and routinely provides the density profile. The infrared (CO_2) laser interferometer has 80 channels for precise density profile measurement. A specific interferometer for electron density fluctuation measurement, a PCI interferometer, is also operating. A millimeter-wave interferometer that measures a divertor plasma is installed to measure dynamics of edge plasmas in detail.

As a laser source for an interferometer and a polarimeter, we have been developing a CH_3OD laser, whose output wavelengths are 57 and 48 μm (Refs. 26 through 29) for high-density discharges. The beam-bending effect will be about one-fourth that of the CH_3OH laser light, and the phase shift is about fivefold larger than that of the CO_2 laser light. Hence, the CH_3OD laser will reduce the fringe jump errors and have high-density resolution. Since the laser can oscillate two wavelengths simultaneously, it can compose a two-color interferometer system intrinsically. The wavelength is also appropriate for the polarimeter from the viewpoints of the amount of the Faraday rotation angle and smallness of coupling effect of the Faraday and the Cotton-Mouton effects, which leads to an error of the Faraday rotation measurement.

ACKNOWLEDGMENTS

These works are supported by the budget ULHH501 and ULHH525 of the National Institute for Fusion Science. The authors are grateful to the LHD operation group for their excellent technical support.

REFERENCES

1. D. VERON, "Submillimeter Interferometry of High-Density Plasmas," in *Infrared and Millimeter Waves*, Vol. 2, pp. 69–135, Academic Press, New York (1979).

2. K. KAWAHATA et al., "A Two Color Millimeter-Wave Interferometer for the Measurement of Line Integral Electron Density on Large Helical Device," *Rev. Sci. Instrum.*, **70**, 695 (1999).

3. K. KAWAHATA et al., "Design and Construction of a Far Infrared Laser Interferometer for the LHD," *Fusion Eng. Des.*, **34–35**, 393 (1997).

4. K. KAWAHATA et al., "Far Infrared Laser Interferometer System on the Large Helical Device," *Rev. Sci. Instrum.*, **70**, 707 (1999).

5. K. TANAKA et al., "Density Reconstruction Using a Multi-Channel Far-Infrared Laser Interferometer and Particle Transport Study of a Pellet-Injected Plasma on the LHD," *Plasma Fusion Res.*, **3**, 050 (2008).

6. K. TANAKA et al., "CO_2 Laser Imaging Interferometer on LHD," *Rev. Sci. Instrum.*, **72**, 1089 (2001).

7. T. AKIYAMA et al., "CO_2 Laser Imaging Interferometer for High Spatial Resolution Electron Density Profile Measurements on LHD," *Rev. Sci. Instrum.*, **74**, 1638 (2003).

8. A. L. SANIN et al., "Imaging Interferometer for Plasma Density Profile and Microturbulence Study on LHD," *Proc. 30th Conf. Controlled Fusion and Plasma Physics*, St. Petersburg, Russia, July 7–11, 2003, ECA Vol. 27A, P-1.73 (2003).

9. K. TANAKA et al., "Precise Density Profile Measurements by Using a Two Color YAG/CO_2 Laser Imaging Interferometer on LHD," *Rev. Sci. Instrum.*, **75**, 3429 (2004).

10. L. N. VYACHESLAVOV et al., "Application of Precise Phase Detector for Density Profile and Fluctuation Measurements Using CO_2 Imaging Heterodyne Interferometer on LHD," *Rev. Sci. Instrum.*, **77**, 10E909 (2006).

11. K. TANAKA et al., "Improvements of CO_2 Laser Heterodyne Imaging Interferometer for Electron Density Profile Measurements on LHD," *Plasma Fusion Res.*, **2**, S1033 (2007).

12. K. TANAKA et al., "Phase Contrast Imaging Interferometer for Edge Density Fluctuation Measurements on LHD," *Rev. Sci. Instrum.*, **74**, 1633 (2003).

13. A. L. SANIN et al., "Two-Dimensional Phase Contrast Interferometer for Fluctuations Study on LHD," *Rev. Sci. Instrum.*, **75**, 3439 (2004).

14. C. A. MICHAEL et al., "Upgraded Two-Dimensional Phase Contrast Imaging System for Fluctuation Profile Measurement on LHD," *Rev. Sci. Instrum.*, **77**, 10E923 (2006).

15. L. VYACHESLAVOV et al., "Instrumental Capabilities and Limitations of Two-Dimensional Phase Contrast Imaging on LHD," *Plasma Fusion Res.*, **2**, S1035 (2007).

16. C. A. MICHAEL et al., "Change of Fluctuation Properties During Non-Local Temperature Rise in LHD from 2d Phase Contrast Imaging," *J. Phys. Conf. Ser.*, **123**, 012018 (2008).

17. C. A. MICHAEL et al., "Detection of High k Turbulence Using Two Dimensional Phase Contrast Imaging on LHD," *Rev. Sci. Instrum.*, **79**, 10E724 (2008).

18. K. TANAKA et al., "Two-Dimensional Phase Contrast Imaging for Local Turbulence Measurements in Large Helical Device," *Rev. Sci. Instrum.*, **79**, 10E702 (2008).

19. C. MICHAEL et al., "Measurements of Micro-Turbulence in High Beta and High Density Regimes of LHD and Comparison with Resistive G-Mode Scaling," *Plasma Fusion Res.*, **3**, S1071 (2008).

20. M. BORN and E. WOLF, *Principles of Optics*, p. 423, Pergamon Press, New York (1959).

21. S. KADO et al., "Improvement of the Laser Phase Contrast Method for Measuring the Spatial Distribution of Electron Density Fluctuations in Heliotron E," *Jpn. J. Appl. Phys.*, **34**, 6492 (1995).

22. J. MIYAZAWA et al., "Self-Sustained Detachment in the Large Helical Device," *Nucl. Fusion*, **46**, 532 (2006).

23. K. TOI et al., "Observation of the Low to High Confinement Transition in the Large Helical Device," *Phys. Plasmas*, **12**, 020701 (2005).

24. Y. ITO et al., "Improved Resolution for a Multi-Fringe Phase Detection Circuit of a Far Infrared Laser Interferometer on LHD," *Fusion Eng. Des.*, **56–57**, 965 (2001).

25. S. MASUZAKI et al., "The Divertor Plasma Characteristics in the Large Helical Device," *Nucl. Fusion*, **42**, 750 (2002).

26. S. OKAJIMA et al., "Development of Short-Wavelength Far-Infrared Laser for High Density Plasma Diagnostics," *Rev. Sci. Instrum.*, **72**, 1094 (2001).

27. K. NAKAYAMA et al., "High-Power 47.6 and 57.2 μm CH_3OD Lasers Pumped by Continuous-Wave 9R(8) CO_2 Laser," *Rev. Sci. Instrum.*, **75**, 329 (2004).

28. K. KAWAHATA et al., "Development of Terahertz Laser Diagnostics for Electron Density Measurements," *Rev. Sci. Instrum.*, **79**, 10E707 (2008).

29. T. AKIYAMA et al., "Short Wavelength Far Infrared Laser Polarimeter with Silicon Photoelastic Modulators," *Rev. Sci. Instrum.*, **79**, 10E720 (2008).